Check for updates

Batteries & Supercaps

Research Article
doi.org/10.1002/batt.202200453

Chemistry Europe
European Chemical Societies Publishing

www.batteries-supercaps.org

Marrying a Non-Flammable Phosphate Solvent with Lithium Nitrate: Novel Electrolyte for Intrinsically Safe and High Performance Lithium Metal Batteries

Hieu Dinh Nguyen,[a] Thuy Duong Pham,[a] Abdullah Bin Faheem,[a] Hye Min Oh,*[b] and Kyung-Koo Lee*[a]

The formation of lithium (Li) dendrites and deterioration of the mechanical integrity of Nickel (Ni)-rich cathodes directly hinder the commercialization of high-voltage Li metal batteries (LMBs) with Ni-rich cathodes. Herein, a novel electrolyte was tailored by combining non-flammable triethyl phosphate (TEP) solvent with easily-synthesized lithium nitrate ($LiNO_3$) as the main salt and fluoroethylene carbonate (FEC) additive. The preferential electrochemical decomposition of $LiNO_3$ and FEC provides robust and conductive solid/cathode electrolyte interphase (SEI/CEI) layer on the surface of the anode/cathode, which can protect both electrodes effectively during long-term cycling. Benefiting from the synergetic effect of $LiNO_3$ and FEC, NFE–$LiNO_3$ exhibited outstanding performances in the cells with $LiNi_{0.6}Mn_{0.2}Co_{0.2}O_2$ (Li||NMC622) under high voltage (4.3 V), achieving an extremely high average efficiency of ~100% with an exceptional capacity retention of 90% after 250 cycles. This study provides useful insights into the rational design of highly efficient, non-flammable, and low-cost electrolyte for long-lasting high-voltage LMBs.

Introduction

Nowadays, climate change and energy security are very hot topics that have gained attention worldwide.[1–6] The decrease in carbon dioxide emissions and use of fossil fuels, in particular, obligates the governments to modulate the automotive industry to manufacture and introduce eco-friendly vehicle, namely electric vehicle (EV), to consumers. The emergence of EV increases the demands for advanced battery techniques with high energy density and cost-effectiveness.[7] So far, lithium-ion batteries (LIBs) with graphite anode (~372 mAh g^{-1} theoretical specific capacity) and lithium transition metal oxide cathode [$LiFePO_4$ (LFP), $LiCoO_2$ (LCO), $LiNi_xMn_yCo_{1-x-y}O_2$, etc.]have been widely used for EV, electronic devices, energy storage, etc.[4–6,8] However, due to their relatively low energy density (≈350 Wh kg^{-1}), the LIB technology fails to meet the expectations for EV development.[9,10] Therefore, much attention has been paid to anodes and cathodes to increase the operation voltages, specific capacities, and energy density of batteries.[7,11] As a promising alternative solution, lithium metal batteries (LMBs) emerge as an ideal candidate since it possesses a higher specific capacity (3860 mAh g^{-1}) than that of the common graphite anode (372 mAh g^{-1}).[4–6,9,12,13] Furthermore, a low redox potential (≈3.040 V vs. standard hydrogen electrode) and high electronic conductivity of Li are beneficial for faster reaction kinetics and an increase in charging speed.[7] Despite the discernible advantages of LMBs, it remains a great challenge to develop practical applications using the LMBs.[9,14] The uncontrollable formation of lithium dendrites during the charging process is an inherent limitation, which has been well-known for a long time. It can reduce the cycle life of batteries and in the worst case, cause an internal short circuit and safety concerns. Furthermore, the high reactivity of traditional electrolytes with Ni-rich cathode materials can also lead to severe side reactions, which induces thermal instability and the serious degradation of cathode capacity under high working voltages (e.g., 4.3 V and above).[11]

Concerning the safety risks, considerable research regarding non-flammable electrolytes such as LHCEs,[10,15–21] ionic liquids,[22–25] solid-state electrolytes,[26,27] and phosphate-based electrolytes[17,28–32] have gained particular attention. Among these, organic alkyl phosphates have been extensively studied as flame-retardant additives (fluorinated alkyl phosphates),[33,34] co-solvent or solvent (e.g., dimethyl methyl phosphonate (DMMP), trimethyl phosphate (TMP), triethyl phosphate (TEP))[17,29,30,35–40] due to their flame-retardant ability and good physicochemical properties (good solubility of Li salts and wide electrochemical stability window). However, the phosphate-based electrolyte at the moderate concentration does not possess good compatibility with Li metal due to the severe side reaction between Li metal and the electrolyte. The high reactivity of the phosphate-based solvent can be suppressed by modification [e.g., high concentrated electrolyte (HCE), additives], and then the electrolyte systems can be compatible with Li metal.[28–30,38] For example, HCEs were fabricated using

[a] H. Dinh Nguyen, T. Duong Pham, A. Bin Faheem, Prof. K.-K. Lee
Department of Chemistry
Kunsan National University
Gunsan, Jeonbuk 54150, Republic of Korea
E-mail: kklee@kunsan.ac.kr
[b] Prof. H. Min Oh
Department of Physics
Kunsan National University
Gunsan, Jeonbuk 54150, Republic of Korea
E-mail: ohmin@kunsan.ac.kr

Supporting information for this article is available on the WWW under https://doi.org/10.1002/batt.202200453

© 2022 Wiley-VCH GmbH

Research Article
doi.org/10.1002/batt.202200453
Chemistry Europe
European Chemical Societies Publishing

phosphate-based solvents, making them become a promising approach for inhibiting the reduction reactions between phosphate-based electrolyte and Li metal.[29,30,38] However, HCEs remain several disadvantages such as high costs, high viscosity, and poor wettability to both electrodes (i.e., cathode and anode). Hence, considerable efforts with the non-flammable phosphate-based solvent are still ongoing to achieve better performance for the LMBs while the salt concentration is reduced to low concentration (i.e.,$\leq$1 M). In addition, a non-flammable LHCE was developed using an "inert" and poorly solvating solvent [i.e., bis(2,2,2,-trifluoroethyl) ether (BTFE)] to dilute the HCE consisting of 3.2 M LiFSI in TEP, which enabled the stable cycling of Li metal anode effectively with a high CE (~99.2%).[17] Recently, a strategy for constructing the nitriding interface via modified phosphate-based electrolytes including lithium nitrate ($LiNO_3$) [1 M LiTFSI in TEP with 2 wt% of vinylene carbonate (VC) and 5 wt% $LiNO_3$] was proved to successfully protect Li metal from the above-mentioned impact of TEP solvent and suppress the formation and growth of Li dendrite.[28]

In this study, we simply fabricated non-flammable phosphate-based electrolytes comprising 1 M different lithium salts (i.e., $LiPF_6$, LiTFSI, $LiNO_3$) in the TEP solvent with 5 wt% FEC as an additive (denoted as NFE–$LiPF_6$, NFE–LiTFSI, NFE–$LiNO_3$, respectively, hereafter). We systematically investigated the effect of salts on the stability of both electrodes and the performance of LMBs. Normally, $LiNO_3$ has been used as a component, mainly an additive in the electrolyte to build a very stable SEI layer comprising inorganic-rich species such as Li_2O, Li_3N, and LiN_xO_y that have much higher ionic conductivity (~10^{-3} S cm^{-1}) than LiF (~10^{-9} S cm^{-1}).[41] This can lead to a uniform and smooth Li deposition on the Li metal anode. In addition, the cost of $LiNO_3$ is lower than that of the other salts (Table S1). The low cost of $LiNO_3$ is the key to decrease the total price of the formulated electrolyte (i.e., NFE–$LiNO_3$) (Table S2). Nevertheless, the solubility of $LiNO_3$ was reported to be extremely low in most carbonate electrolytes due to the lower Gutmann donor number (DN) of carbonate solvents [e.g., EC (~16), DMC (~17), PC (~15)] than that of NO_3^- (~22).[42] Hence, several efforts have been made to increase the amount of $LiNO_3$ in cells with carbonate-based electrolytes. For instance, introducing $LiNO_3$ particles into porous glass fiber as separators or coating layers on the surface of Li metal anode.[43,44] The other method is the employment of $LiNO_3$ solubilizers with higher DN like γ-butyrolactone, dimethyl sulfoxide, and sulfolane to increase the solubility of $LiNO_3$, and then a small fraction of the mixture was added as an additive into the carbonate-based electrolytes.[45–47] The latter was demonstrated to be more facile and successful in forming very stable SEI layers on the Li metal, enabling high-voltage LMBs with superior performance. However, considering an additional manufacturing process (i.e., solubilizing a large amount of $LiNO_3$ into a high-DN solvent), the commercialization of $LiNO_3$ containing electrolytes would be challenging. Furthermore, the high interaction energy between Li^+ and NO_3^- can significantly influence the physical and electrochemical properties of the designed electrolyte. Therefore, it is crucial to develop an electrolyte containing only $LiNO_3$ as the main salt to fully exploit the advantageous effects of $LiNO_3$ in enhancing the Li plating/stripping cycles and decreasing the total cost of the electrolyte.

Herein, we propose novel-tailored electrolyte composed of 1 M $LiNO_3$ in the TEP solvent with 5 wt% FEC as an additive. TEP was chosen as the organic solvent because of its higher solubility of $LiNO_3$ (the saturation concentration is 2.5 M at 25 °C) (see Figure S1) as well as non-flammability. Furthermore, the synergetic effect of the $LiNO_3$ and FEC additive in NFE–$LiNO_3$ results in an electrolyte system capable of restraining the highly chemical reactivity of TEP to Li metal, suppressing the growth of Li dendrite to the Li metal anode, and quenching parasitic reactions between the electrolyte and the Ni-rich cathode material under high operation voltage (up to 4.3 V). As a result, a high average CE (~97.23%) in the Li||Cu cells and a small polarization (~110 mV) in the Li||Li symmetric cells were obtained. Moreover, in LMB cells with Ni-rich cathode (Li||NMC622) under 4.3 V, the proposed electrolyte (NFE–$LiNO_3$) exhibited an extremely high average efficiency of ~100% and a high capacity retention of 90% after 250 cycles.

Results and discussion

Physicochemical properties of the electrolytes

An electrolyte system with high solubility of the main salt normally regulates the physical or electrochemical property by varying the concentration of the electrolyte. Generally, in the electrolyte the interaction between the cation and anion must be weakened to increase the salt dissociation, meaning that the interaction between ions and solvents must exceed the interaction between cations and anions.[47] Due to the strong interaction between Li^+ cation and NO_3^- anion, $LiNO_3$ cannot be well-dissolved in the common solvent for the electrolytes (e.g., carbonate electrolytes). However, herein, the solubility issue can be overcome using the TEP solvent, a solvent with a high ability to dissolve lithium salts (i.e., high DN),[48] resulting in a high salt dissolving capability (saturation point is 2.5 M at 25 °C). Furthermore, compared with the other solvents (e.g., 1,2-dimethoxyethane, sulfolane) with the ability to solubilize $LiNO_3$, the ionic conductivity of $LiNO_3$ in TEP is significantly higher (see Figure S2). This further proves that TEP is one of the most suitable candidates for LMB electrolytes due to its notable physical properties such as low melting point (−56.5 °C), high dielectric constant (13), and high DN (26).[48,49] The ionic conductivity and viscosity of the NFE–$LiNO_3$, NFE–$LiPF_6$, and NFE–LiTFSI were determined and are shown in Figure 1(a). The ionic conductivity values were 2.76 mS cm^{-1} (NFE–$LiNO_3$), 6.36 mS cm^{-1} (NFE–$LiPF_6$), and 4.79 mS cm^{-1} (NFE–LiTFSI). Those values were comparable to the previous literatures, and were high enough to meet the requirements for LMB application.[17,31,32] The low ionic conductivity of NFE–$LiNO_3$ compared with the others might be correlated with a large number of CIPs and AGGs present in the electrolyte.[5]

© 2022 Wiley-VCH GmbH

25666223, 2023, 2, Downloaded from https://chemistry-europe.onlinelibrary.wiley.com/doi/10.1002/batt.202200453 by University of Ulsan, Wiley Online Library on [11/11/2025]. See the Terms and Conditions (https://onlinelibrary.wiley.com/terms-and-conditions) on Wiley Online Library for rules of use; OA articles are governed by the applicable Creative Commons License

Research Article
doi.org/10.1002/batt.202200453
Chemistry Europe
European Chemical Societies Publishing

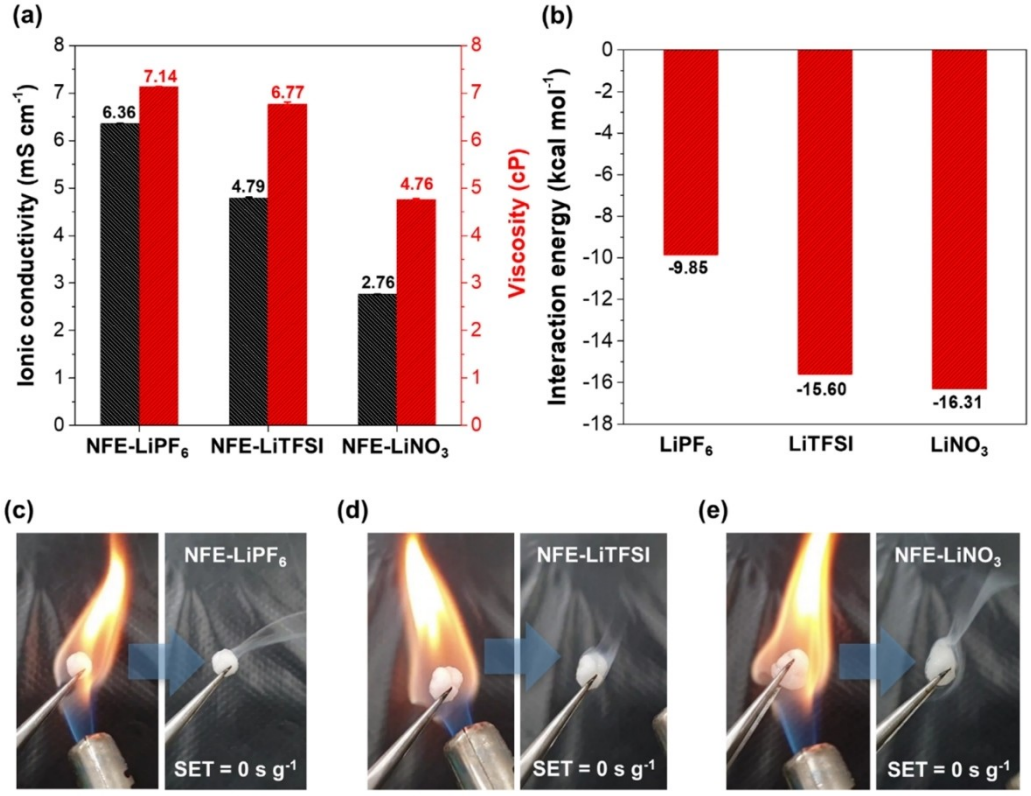

Figure 1. a) Ionic conductivity and viscosity of NFE–$LiPF_6$, NFE–LiTFSI, and NFE–$LiNO_3$ at 25 °C. b) Interaction energies of different salts were obtained by DFT calculations. Flammability tests for c) NFE–$LiPF_6$, d) NFE–LiTFSI, and e) NFE–$LiNO_3$.

Furthermore, among the other salts in this study, $LiNO_3$ exhibits the strongest interaction energy in TEP according to DFT calculation results. Thus, the free ions might be difficult to be generated in solution (see Figure 1b). On the other hand, vast cation-anion-associated complexes in an electrolyte system, on the other hand, can form a stable SEI layer via the preferential reduction reaction on the anode.[4–6] Generally, cell kinetics can be determined by surface chemistry and ionic conductivity. Although NFE–$LiNO_3$ possesses low ionic conductivity relative to the others investigated here, it can form the best passivation layers with low resistance on the electrode surface, resulting in the best electrochemical performance (will be addressed later). The investigation of ionic conductivity along with the increasing concentration of the $LiNO_3$ in TEP was performed. The ionic conductivity increased then decreased after reaching a maximum (see Figure S1a). Interestingly, the highest ionic conductivity was maintained at 1 M. Furthermore, the viscosity increases along the $LiNO_3$ concentration is associated with the rise in the total interactions between the molecules, especially the charge species, while the characteristic trend of ionic conductivity can be explained by the limitation of the number of free ions, which have been regarded as effective charge carriers.[6] The t_{Li^+}, which represents the contribution of Li^+ to the total ionic conductivity, was determined and is shown in Figure S1b. NFE–$LiNO_3$ possessed t_{Li^+} of 0.623, which was higher than that of NFE–$LiPF_6$ and NFE–LiTFSI with values of 0.523 and 0.308, respectively. When the electrolyte has a t_{Li^+} higher than 0.5, cation motion contributes more to the total ionic conductivity than the anion.[50] The higher t_{Li^+} of NFE–$LiNO_3$ also indicates that NFE–$LiNO_3$ can decrease the concentration polarization and side reactions with electrodes, especially suppress the formation of dendrites on the surface of the Li metal anode.[5,51]

In order to investigate the solvation characteristics of 1 M $LiPF_6$, 1 M LiTFSI, and 1 M $LiNO_3$ in TEP (denoted as $LiPF_6$-TEP, LiTFSI-TEP, and $LiNO_3$-TEP, respectively), Raman spectroscopy was employed. The ionic speciation of $LiPF_6$ and LiTFSI in various electrolyte systems has been studied in the frequency range of 720–760 cm^{-1}, where the S–N–S and F–P–F symmetric stretching vibration mode of the $TFSI^-$ and PF_6^-, respectively, can be observed.[52,53] However, an in-depth study of the solvation structure of the electrolyte containing $LiNO_3$ as the main salt is highly required to understand the ionic speciation in the electrolyte. Thus, the solvation structure was studied along with the concentration of $LiNO_3$ in the frequency range of 1010–1065 cm^{-1}, in which the O–N–O symmetric vibration mode of the NO_3^- anion can be observed.[54] The Raman spectra were deconvoluted into four different Gaussian-Lorentz (Voigt) functions related to the different cation-anion coordination structures in TEP. The bands at ~1038 cm^{-1} (red solid line), ~1042 cm^{-1} (blue solid line), ~1048 cm^{-1} (pink solid line), ~1056 cm^{-1} (dark yellow solid line) are assigned to free anions, CIP (NO_3^- coordinating to one Li^+), AGG–I (NO_3^- coordinating to two Li^+), and AGG-II (NO_3^- coordinating to more than two

© 2022 Wiley-VCH GmbH

25666223, 2023, 2, Downloaded from https://chemistry-europe.onlinelibrary.wiley.com/doi/10.1002/batt.202200453 by University of Ulsan, Wiley Online Library on [11/11/2025]. See the Terms and Conditions (https://onlinelibrary.wiley.com/terms-and-conditions) on Wiley Online Library for rules of use; OA articles are governed by the applicable Creative Commons License

Li^+), respectively (Figure S3). In order to confirm the assignments of Raman spectra, the DFT calculations (B3LYP/6-311G++) were conducted with the initial structures of the solvates extracted from First Principles Molecular Dynamics (FPMD) simulation snapshots (see below) of the $LiNO_3$-TEP electrolyte (Figure S4). The calculated frequencies are tabulated in Table S3.[55] The trend for the increasing frequencies in the theoretical calculation was similar to the experimental values, following this order: free anions < CIP < AGG–I < AGG-II. The percentage of ionic speciation was calculated by dividing the area of each peak by the total area of all peaks. In general, the free anions in diluted systems will dominate, then decrease as the concentration increases, herein, the same trend was observed (e.g., 54.55% at 0.125 M and 9.17% at 2.5 M) as presented in Figure S5. However, even at a very low concentration such as 0.125 M, considerable CIPs (37.37%) and AGG–I (8.08%) forms can be found, due to a strong cation-anion interaction, resulting in the lack of free Li^+ and free NO_3^-, which further explains the low ionic conductivity of $LiNO_3$ in TEP as above discussion. As the concentration of $LiNO_3$ increases, more associated complexes such as CIPs, AGG–I, and AGG-II will appear.[6] The answer lies in the fact that it is difficult to separate the Li^+ and NO_3^- ions at high concentration due to the insufficiency of TEP molecules, leading to the formation of more aggregated forms such as AGG–I, AGG-II (one anion coordinates with two or more Li^+ cations). As shown in Figure S6, the number of associated complexes of 1 M $LiNO_3$-TEP was higher than that of other electrolytes in this study (i.e., $LiPF_6$-TEP, LiTFSI-TEP), and a small amount of AGG-II species existing in $LiNO_3$-TEP (~2.92%) was also obtained. Furthermore, the number of free anions decreases as follows: $LiPF_6$-TEP (46.14%) > LiTFSI-TEP (30.48%) > $LiNO_3$-TEP (19.76%), which is consistent with the trend obtained from MD simulation (see below).

In order to further investigate the effect of the salt on the solvation structures in studied electrolytes, classical molecular dynamics (CMD) simulations were conducted (see Tables S4–S6). The heights of the first peaks of the radial distribution functions (RDF) in Figure S7 show the probability of finding an anion/solvent molecule in the primary solvation sheath of Li^+. From the first peak of the Li^+ - NO_3^- RDF in Figure S7(c), it can be observed that the degree of Li^+ - NO_3^- interactions are significantly greater than that of Li^+ - TEP. In contrast, the first peaks of the Li^+ - Anion RDFs in $LiPF_6$-TEP (Figure S7a) and LiTFSI-TEP (Figure S7b) are lower than Li^+ - TEP. Hence, from the RDFs, it was seen that NO_3^- has a stronger preference for interacting with Li^+, in comparison to PF_6^- and $TFSI^-$. From the average coordination numbers (CNs) (Figure S8a) of anions in the first coordination shell of Li^+, the Li^+ - anion CNs increase in the following order: $LiPF_6$-TEP (0.14) < LiTFSI-TEP (0.42) < $LiNO_3$-TEP (1.40). Since the Li^+ - anion CNs in $LiNO_3$-TEP is between 1.0 and 2.0, this implies that a large fraction of Li^+ is surrounded by 1 or 2 NO_3^- anions. Furthermore, it can be observed that the number of free anions in their first coordination shell decrease in the order: $LiPF_6$-TEP (86.2%) > TFSI-TEP (61.0%) > $LiNO_3$-TEP (2.9%) (Figure S8b). This follows the same trend as observed in the Raman spectra. The greater tendency of CIPs and AGGs formation in $LiNO_3$-TEP is also evident from the percentage of anions with a particular number of Li^+ in their first coordination shell. It can be seen that the fraction of NO_3^- in $LiNO_3$-TEP that are surrounded by one (CIPs) or more (AGGs) Li^+ is 57.6% and 37.4%, respectively. In summary, the MD simulation also shows that the degree of cation-anion interactions in $LiNO_3$-TEP is relatively high, leading to the formation of associated complexes (such as CIPs and AGGs) in the electrolyte system.

To characterize the flammability of the electrolytes used in this study, self-extinguishing time (SET) tests were carried out. As shown in Figure 1(c), all the electrolytes did not catch fire from a torch even when the ignition source was removed, and all showed a zero SET value (0 s g^{-1}). The excellent non-flammable characteristic of the electrolytes in our study can be explained by the presence of TEP solvent, which operates via the radical trap mechanism (see Supporting Information).

Intrinsic electrochemical stability of the electrolytes

Linear sweep voltammetry (LSV) measurements were performed to investigate the electrochemical stability of all electrolytes (Figure S9). All electrolytes showed higher onset oxidation potential values than the operation voltage of most cathode materials (~5.8, 5.2, 4.9 V for NFE–$LiPF_6$, NFE–LiTFSI, NFE–$LiNO_3$, respectively), indicating that they can be applied to high-voltage LMBs. Furthermore, NFE–$LiNO_3$ exhibited a narrower electrochemical stability window (ESW) with a lower onset oxidation potential and a higher onset reduction potential than the other electrolytes. In previous studies, $LiNO_3$ and FEC have been used as functional additives to stabilize the Li metal anode. Due to the higher reduction potential of $LiNO_3$, it can be expected to reduce first, forming Li_2O, Li_3N, and LiN_xO_y species in the SEI layer.[46,47,56,57] Additionally, the LiF species generated from the reduction of FEC additive has also been regarded as one of the most important components to build a stable SEI layer.[47,58] The preferential reduction of $LiNO_3$ and FEC enables the formation of a strong SEI layer consisting of the various inorganic species (i.e., LiF, Li_2O, Li_3N, and LiN_xO_y) on the surface of the Li metal anode. The inorganic species have higher interfacial energy with Li metal anode than the organic species, which can inhibit the formation and growth of Li dendrite.[46] According to the LSV measurements, the reduction reaction happened sequentially, wherein the onset reduction potential of $LiNO_3$ and FEC was determined to be ~1.7 V and ~1.0 V vs. Li/Li^+, respectively, similar to the values obtained in the previous studies.[56,58] To verify the reason for the behavior of the reduction/oxidation reaction, the DFT calculations were performed and are presented in Figure S10. In general, the molecule exhibiting the lowest LUMO energy will reduce first, dominating the formation of the SEI layer.[59] According to the molecular orbital profiles, among the chemical species in NFE–$LiNO_3$ electrolyte, the reduction of $Li^+\cdots NO_3^-$ can happen first owing to the lowest LUMO energy level. Successively, $Li^+\cdots$FEC can be reduced due to the lower LUMO energy level than the TEP solvent. The order of the reduction reaction is similar to

© 2022 Wiley-VCH GmbH

25666223, 2023, 2, Downloaded from https://chemistry-europe.onlinelibrary.wiley.com/doi/10.1002/batt.202200453 by University of Ulsan, Wiley Online Library on [11/11/2025]. See the Terms and Conditions (https://onlinelibrary.wiley.com/terms-and-conditions) on Wiley Online Library for rules of use; OA articles are governed by the applicable Creative Commons License

Research Article
doi.org/10.1002/batt.202200453
Chemistry Europe
European Chemical Societies Publishing

that observed in the LSV measurement. Furthermore, NFE–$LiNO_3$ exhibited a lower onset oxidative potential than the others (Figure S9), which can be inferred to the preferential electrochemical oxidation of $LiNO_3$ and FEC on the electrode surface. This was verified by DFT calculation, wherein the highest occupied molecular orbital (HOMO) energy level of Li^+···NO_3^- and FEC was found to be higher than the other chemical species. From a thermodynamic viewpoint, the higher the HOMO level is, the oxidation reaction is easier to occur. As shown in Figure S10, the HOMO energy of Li^+···NO_3^- is higher than that of Li^+···PF_6^- and Li^+···$TFSI^-$ in TEP, indicating that Li^+···NO_3^- is easy to be oxidized compared to Li^+···PF_6^- and Li^+···$TFSI^-$. This is in agreement with the study reported by Phiri et al., in which $LiNO_3$ was used as an additive in the carbonate-based electrolyte, and it can be oxidized first on the surface of the cathode electrode to protect it from the parasitic reactions with the electrolyte.[56] These results indicate that the synergetic effect of $LiNO_3$ and FEC (i.e., the preferential reduction/oxidation reaction) was associated with the formation of a stable SEI/CEI layer on the Li metal anode/Ni-rich NMC cathode (will be discussed later).

Furthermore, the preferential decomposition of NO_3^- in $LiNO_3$-TEP was also observed from the calculated projected density of states (PDOS) of $LiPF_6$, LiTFSI, and $LiNO_3$ in TEP. Figure 2 shows the PDOS of snapshots obtained from FPMD simulations (see Supporting Information). From Figure 2, it can be observed that NO_3^- dominates the frontier orbitals in $LiNO_3$-TEP, implying the preferential reduction and oxidation of NO_3^-. This leads to the formation of dense and stable SEI/CEI layers that are rich in inorganic species (Li_2O, Li_3N, and LiN_xO_y). In comparison, for $LiPF_6$-TEP and LiTFSI-TEP, the HOMO and/or LUMO orbitals are occupied by both the anion and solvent molecules. Therefore, the solvent molecules can decompose more readily, resulting in unstable SEI and CEI layers that contain organic components. The relatively smaller ESW of $LiNO_3$-TEP from LSV measurements (Figure S9) is observed in the PDOS calculation as well. The difference in energy between the HOMO and LUMO orbitals in $LiNO_3$-TEP (Figure 2c) is noticeably smaller compared to $LiPF_6$-TEP (Figure 2a) and LiTFSI-TEP (Figure 2b). Hence, NO_3^- acts as an important species, and the benefits of its preferential reduction/oxidation in the formation of stable SEI/CEI layer are evident from experimental and theoretical results.

Cycling performance of lithium metal anode in studied electrolytes

The Li||Cu coin cells were used to evaluate the cycle stability of Li plating/stripping with the electrolytes used in this study, and the average CEs were obtained using method 3 reported by Adams et al.[60] Among the values obtained from Li||Cu coin

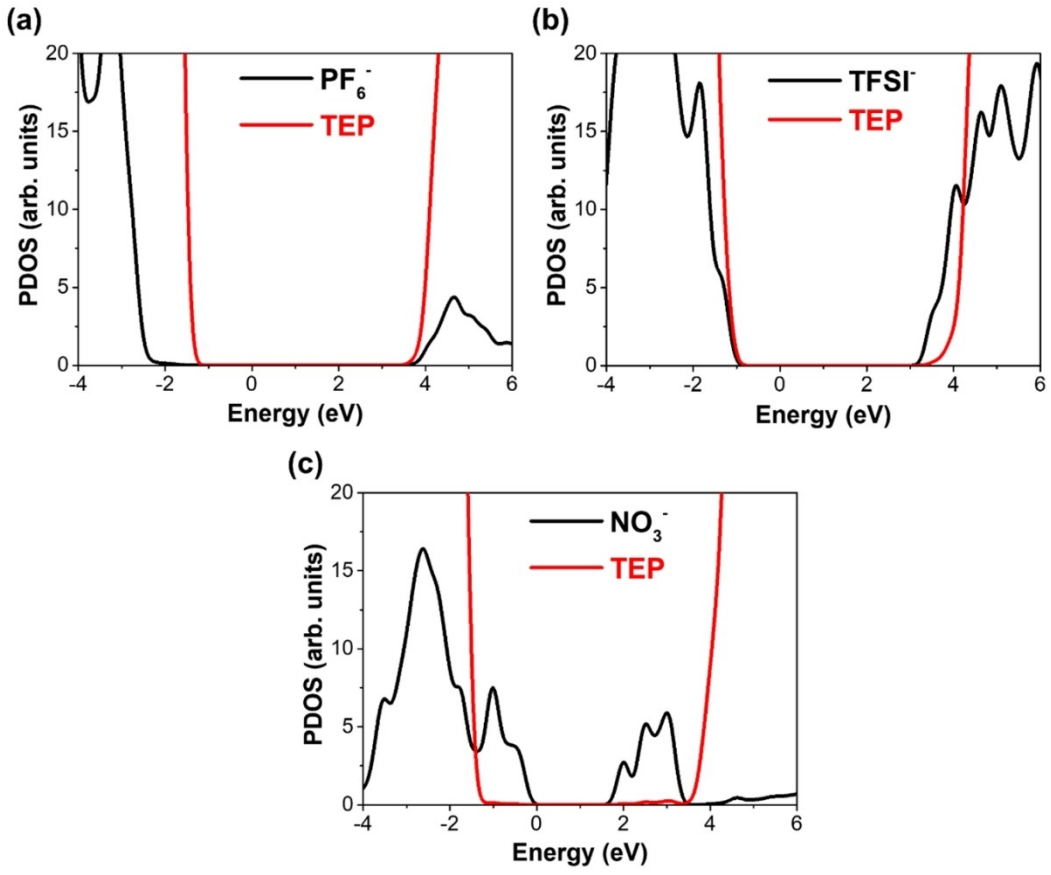

Figure 2. Projected density of states (PDOS) obtained from FPMD simulations for the a) $LiPF_6$-TEP, b) LiTFSI-TEP, and c) $LiNO_3$-TEP electrolyte systems.

© 2022 Wiley-VCH GmbH

25666223, 2023, 2, Downloaded from https://chemistry-europe.onlinelibrary.wiley.com/doi/10.1002/batt.202200453 by University of Ulsan, Wiley Online Library on [11/11/2025]. See the Terms and Conditions (https://onlinelibrary.wiley.com/terms-and-conditions) on Wiley Online Library for rules of use; OA articles are governed by the applicable Creative Commons License

cells, the best CEs of the NFE–$LiPF_6$, NFE–LiTFSI, and NFE–$LiNO_3$ were 92.1%, 92.5%, and 97.2%, respectively. The highest CE value of NFE–$LiNO_3$ suggests that this electrolyte exhibits good compatibility and limited parasitic reactions with Li metal anode. Importantly, this value is higher than the results obtained for carbonate-based electrolytes. For example, an average CE value of 95.2% for 1 M $LiPF_6$ + 0.15 M lithium difluorophosphate (LiDFP) in EC/DEC (1:1 by volume ratio) was obtained, as reported by Shi et al.[51] Tan et al. also reported a value of 97.3% for TEP-based electrolyte containing 1 M LiTFSI and 2 wt% VC and 5 wt% $LiNO_3$,[28] which was comparable to the CE value of NFE–$LiNO_3$ in our study. Figure S11 shows that the overpotential during the Li plating process can be divided into two parts: i) nucleation overpotential and ii) growth overpotential.[61] In NFE–$LiNO_3$, the nucleation overpotential (defined as the sharp tip at the nucleation stage), which must overcome the Li nucleation barrier on Cu substrates,[11,47] was smallest (~79 mV) among the other electrolytes. It suggests that the Li deposition can be controlled at the nucleation stage in NFE–$LiNO_3$.[47] After that, the voltage goes up to a relatively stable voltage platform, defined as growth overpotential. The growth overpotential is the energy required for the migration of Li-ion to the electrode surface, and it exists throughout the process of Li plating.[62] A smaller growth overpotential (~61 mV) was obtained by NFE–$LiNO_3$ over NFE–$LiPF_6$ and NFE–LiTFSI (~89 and 167 mV, respectively), demonstrating that the electrochemical kinetics can be enhanced and uniform Li deposition can be achieved with NFE–$LiNO_3$.[63] The results clearly proved that Li-ion conductive SEI layer which might be from the preferential reduction of $LiNO_3$ and FEC as discussed in LSV measurement (Figure S9) was formed on the electrodes.

To further examine the stability of the Li metal in the investigated electrolytes, cycling tests with symmetric Li||Li coin cells were implemented. A current density of 0.5 mA cm^{-2} and a capacity of 1 mAh cm^{-2} were applied. As seen in Figure 3(b), the stability of the Li||Li cells in the NFE–$LiPF_6$ and NFE–LiTFSI was less than the one obtained in NFE–$LiNO_3$. The synergetic effect of $LiNO_3$ and FEC (i.e., the reduction of associated complexes in NFE–$LiNO_3$ and FEC additive) might be beneficial for enhanced performance of Li metal, as displayed by a small voltage polarization (~110 mV) and a prolonged cycling life up to over 200 h. In contrast, the polarization of NFE–$LiPF_6$ and NFE–LiTFSI was larger (384 and 316 mV, respectively), and the Li||Li cells suffered from short circuits after 125 and 110 h, respectively, as evidenced by a drastic increase in polarization. The poor cycling life was inferred to the dendrite formation on the Li metal surface due to the unstable SEI layer.[4] These results again confirm that NFE–$LiNO_3$ can improve the cycling stability of Li metal anode because of the formation of a robust SEI layer, which prevents side reactions and protects the Li electrodes.

EIS of Li||Li symmetric cells was performed to investigate the stability and compatibility of NFE–$LiNO_3$ over NFE–$LiPF_6$ and NFE–LiTFSI. At first, the resistances of the cells were measured after standing for a certain period (0, 1, 12, 24, 48, 72, 96 h) (Figure S12). The equivalent circuit used to fit the EIS

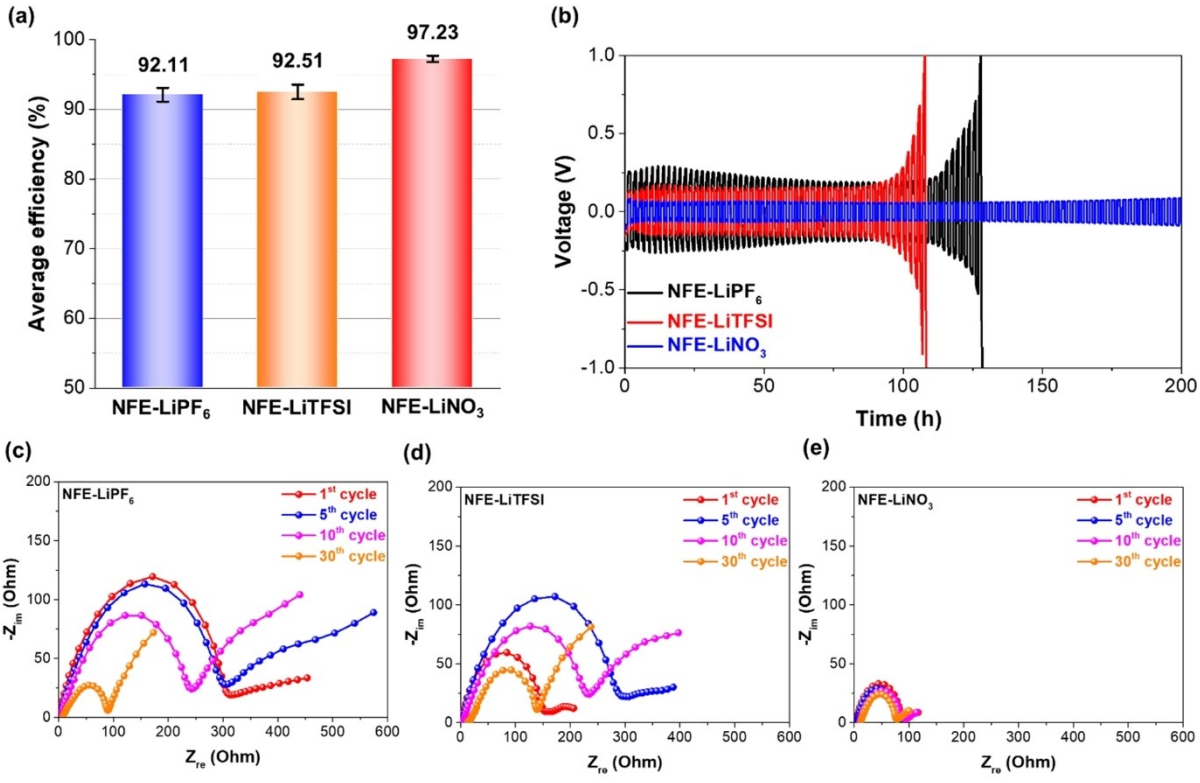

Figure 3. a) Average CE of Li||Cu cells and b) cycling performance of Li||Li symmetric cells at the current density of 0.5 mA cm^{-2} with a capacity of 1 mAh cm^{-2}. Nyquist plot of Li||Li symmetric cells with c) NFE–$LiPF_6$, d) NFE–LiTFSI, e) NFE–$LiNO_3$ after different cycles.

© 2022 Wiley-VCH GmbH

25666223, 2023, 2, Downloaded from https://chemistry-europe.onlinelibrary.wiley.com/doi/10.1002/batt.202200453 by University of Ulsan, Wiley Online Library on [11/11/2025]. See the Terms and Conditions (https://onlinelibrary.wiley.com/terms-and-conditions) on Wiley Online Library for rules of use; OA articles are governed by the applicable Creative Commons License

is illustrated in Figure S13. As reported by Quin et al., the chemical stability of the Li metal-electrolyte interface can be evaluated with the evolution of the SEI layer resistance (R_{SEI}) along with the increase of standing time.[64] After 24 h, the cell with NFE–$LiNO_3$ exhibited a lower R_{SEI} (~160 Ω) than that of the cells with NFE–$LiPF_6$ and NFE–LiTFSI (~209 and ~1002 Ω, respectively). The R_{SEI} values of the NFE–$LiPF_6$ and NFE–LiTFSI kept increasing over 72 h, whereas that of the cell with NFE–$LiNO_3$ did not change significantly, suggesting high chemical stability of NFE–$LiNO_3$ electrolyte with Li metal. Moreover, to explain the high average CE in Li||Cu cells and enhanced cycling performance of Li||Li symmetric cell with NFE–$LiNO_3$, the EIS measurements of cells was performed after different cycles. The Nyquist plots for NFE–$LiPF_6$, NFE–LiTFSI, and NFE–$LiNO_3$ were achieved from the EIS data and are illustrated in Figure 3(c–e), respectively. Herein, the R_{SEI} and the charge transfer resistance (R_{CT}) were used to inspect the resistance of the SEI film forming on Li metal and the charge transfer. The R_{SEI} and R_{CT} values of NFE–$LiPF_6$ and NFE–LiTFSI were highly fluctuated after the 1st cycle, indicating that the formation of the SEI layer required more cycles and might consume more electrolytes. Unlike that, in the case of NFE–$LiNO_3$, small R_{SEI} and R_{CT} values and negligible change of those values were found after the 1st cycle, highlighting the role of both $LiNO_3$ and FEC in the formation of a very stable SEI layer. This result is consistent with the small polarization (~110 mV) of the Li||Li symmetric cell (Figure 3b). The reason for this behavior can be explained by the presence of high Li-ion conductive inorganic species (LiF, Li_2O, Li_3N, and LiN_xO_y) generated from the preferential reduction of $LiNO_3$ and FEC, constructing a stable and low-impedance SEI layer on the Li metal surface (will be discussed later). Thus, those inorganic species can provide channels for faster Li^+ diffusion in the SEI layer, enhancing the kinetics of the Li plating/stripping process, as previously reported by Wang et al.[41] Even though NFE–$LiNO_3$ does not possess high ionic conductivity (Figure 1a), which might cause a degradation of the electrochemical performance of LMBs, the cell kinetics can still be improved more by the sound passivation layer formed in NFE–$LiNO_3$. In other words, surface chemistry can affect cell performance more than bulk conductivity.

Protection of Al corrosion with the investigated electrolyte

To understand the effect of all studied electrolytes on the anodic corrosive behavior of the Al current collect, LSV measurements and subsequently, chronoamperometry (CA) was performed, in which an Al foil was used as the working electrode and Li metal was used as both the counter and reference electrode. It was found that the anodic Al corrosion in all electrolytes occurred at earlier potentials than the oxidation potential determined by the LSV measurement with the Pt working electrode (~3.75, 3.40, 3.25 V for NFE–$LiPF_6$, NFE–LiTFSI, NFE–$LiNO_3$) (see Figure S14). However, the current was stable for all three investigated electrolytes in the CA test (Figure S14b), confirming that the Al corrosion might be suppressed using TEP-based electrolytes designed in this study. The reason behind this protection may come from the formation of a strong passivation layer on the Al surface, which originates from the decomposition of TEP solvent. This layer can reduce the direct contact between the electrolyte and Al, thereby further restraining Al corrosion.[31] However, a different intensity of anodic current during the holding time was observed in the case of investigated electrolytes (Figure S14b), suggesting that the type of salt affected the inhibition of the Al corrosion significantly. The intensity of the anodic current increased in the order: NFE–$LiNO_3$ < NFE–$LiPF_6$ < NFE–LiTFSI. It's a well-known issue when imide salt (e.g., LiFSI or LiTFSI) is employed in the electrolyte.[65,66] Furthermore, the subsequent scan after the 1st in the LSV measurement can give a clearer explanation of the prevention of the Al corrosion in the studied electrolytes. The anodic Al corrosion in all electrolytes with or without FEC additive was extended to a higher potential (≈5.0 V) at the second scan (Figure S14c and d). Since there was no contribution of FEC to the protection of Al corrosion, the passivation layer consisting of the P-containing species (i.e., polyphosphate or $LiPO_x$) formed from the decomposition of TEP solvent will be mainly involved in the inhibition of Al corrosion. The passivated Al foil can avoid corrosion even in the electrolyte containing imide salt (i.e., NFE–LiTFSI) used in this study. Further evidence can be observed in the SEM images (Figure S15), where the Al surface was well-maintained in the studied electrolytes. Above all, these results further indicate that the merit of using TEP as the main solvent lies in not only preventing the flammability but also protecting the Al from anodic corrosion.

Cell performance with high-voltage NMC622 cathode in the studied electrolytes

Coin cells using a Li metal anode and NMC622 cathode at an areal capacity of 0.9 mAh cm^{-2} were assembled and evaluated with the cycling tests to verify the effectiveness of the studied electrolytes for LMB application. Figure 4(a) shows a dramatic difference in the efficiency and discharge capacity between the investigated electrolytes. A fluctuation in the efficiency accompanied by a dramatically fast drop of the discharge capacity (~8% after 100 cycles) can be found in both cells with NFE–$LiPF_6$ and NFE–LiTFSI. The inferior cell performance might be caused by the serious side reactions between the electrodes and the electrolyte, such as the Li dendrite growth on the Li metal surface and the degradation of the NMC622 cathode. In contrast, a high and stable average CE (~100%) with a capacity retention of ~90% after 250 cycles were obtained in the Li||NMC622 cell with NFE–$LiNO_3$, exhibiting superior cycling stability. These results indicate that the cell with NFE–$LiNO_3$ can well protect Li metal and preserve NMC622 structure integrity, hence, boosting the electrochemical performance. Moreover, the voltage profiles of the Li||NMC622 cells at certain cycles during the cycling test were illustrated in Figure S16. The continuous fading of specific capacity accompanied by a large polarization was observed in the voltage profile of cells

© 2022 Wiley-VCH GmbH

25666223, 2023, 2, Downloaded from https://chemistry-europe.onlinelibrary.wiley.com/doi/10.1002/batt.202200453 by University of Ulsan, Wiley Online Library on [11/11/2025]. See the Terms and Conditions (https://onlinelibrary.wiley.com/terms-and-conditions) on Wiley Online Library for rules of use; OA articles are governed by the applicable Creative Commons License

Research Article
doi.org/10.1002/batt.202200453
Chemistry Europe
European Chemical Societies Publishing

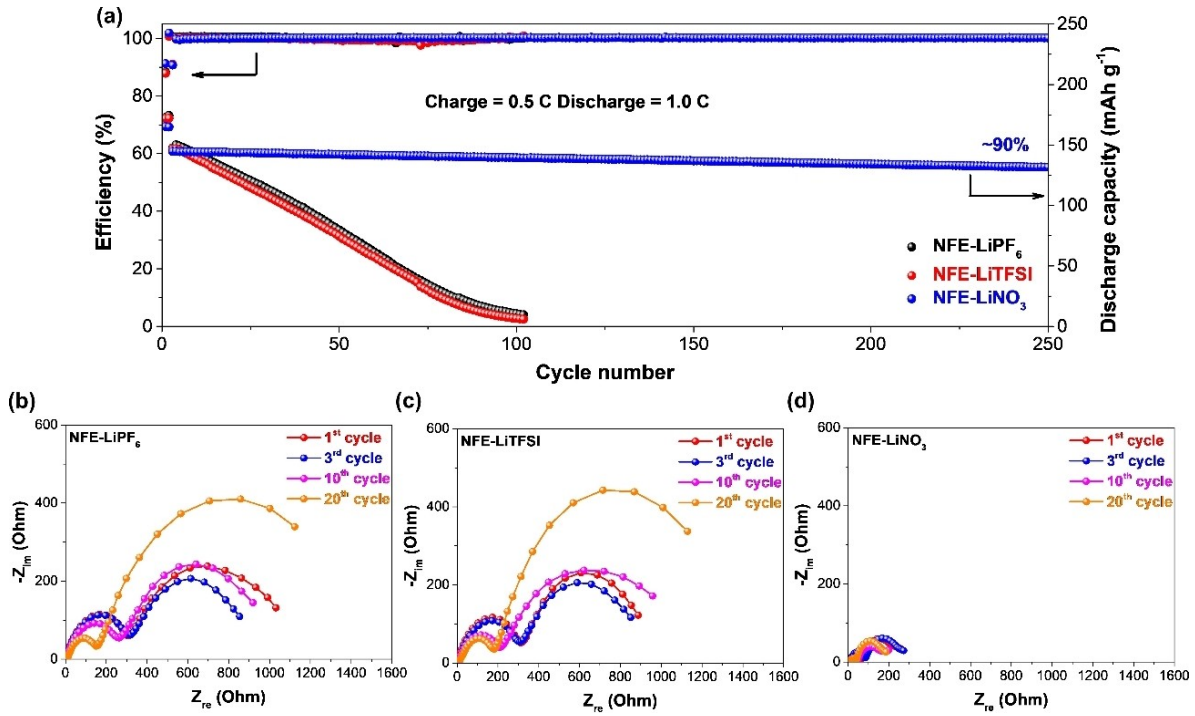

Figure 4. a) Cycling performance of Li||NMC622 cells in NFE–$LiPF_6$, NFE–LiTFSI, NFE–$LiNO_3$. Nyquist plot of Li||NMC622 cells with b) NFE–$LiPF_6$, c) NFE–LiTFSI, d) NFE–$LiNO_3$ after different cycles.

employing NFE–$LiPF_6$ and NFE–LiTFSI prior to a failure after 100 cycles. On the contrary, an outstanding cycling performance of the cell with NFE–$LiNO_3$ was evidenced by a slow decrease in capacity and a smaller polarization even after 250 cycles (see Figure S16a–c). The improved electrochemical performance (i.e., a high average CE and capacity retention) of LMB cells with NFE–$LiNO_3$ was further compared with the previously reported non-flammable electrolytes (Table S7). The synergetic effect of $LiNO_3$ and FEC on the Ni-rich NMC cathode (i.e., the preferential oxidation of $Li^+\cdots NO_3^-$ and FEC), which was revealed in the LSV measurement (Figure S9) and DFT calculation (Figure S10), was beneficial to build a robust, protective CEI layer, which will be further verified by surface analysis in the later sections. This CEI layer plays a vital role in alleviating the unwanted reactions of the electrolyte on the NMC cathode, consequently protecting the NMC crystal lattice.[20] Additionally, the compatibility of NFE–$LiNO_3$ in LMB application was also discovered by coupling the electrolyte with commercial 4 V class cathode materials (e.g., NMC333 and LMO). After 250 cycles, high average CEs (~100%) and capacity retention of ~88% and 100% can be obtained for the Li|| NMC333 and Li||LMO cells, respectively (see Figure S17). The advantages of outstanding protective layers (SEI/CEI) formation and the unique properties of the phosphate-based solvent enabled by NFE–$LiNO_3$ contribute to the adequate suppression of the unwanted reactions, consequently leading to remarkably improved cycling performance.

Inspired by the superior cycling stability of Li||NMC622 cells benefiting from NFE–$LiNO_3$, further exploration of the rate performance of Li||NMC622 cells was also carried out at different charge/discharge current densities (denoted as C-rate). The discharge capacities of the Li||NMC622 under various charge/discharge current densities were compared and are shown in Figure S18. It can be seen that there is a negligible difference in the discharge capacities at the lowest C-rate (0.1 C). However, a stark difference in the rate performance was observed when the C-rate was increased. For instance, when the C-rate reached 5 C, the discharge capacity of the cell with NFE–$LiNO_3$ was ~50 mAh g^{-1}, while a huge drop of capacity was observed with the cells containing NFE–$LiPF_6$ and NFE–LiTFSI (~2.5 and 1.5 mAh g^{-1}, respectively). Moreover, only the NFE–$LiNO_3$ cell can recover to the original value after rate performance tests (i.e., at 0.1 C) and remain stable. It was found that the rate performance of the cell was not strongly affected by the ionic conductivity of the electrolyte included in the cell since the surface chemistry can affect more cell performances than the bulk ionic conductivity, as aforementioned. The enhanced rate performance is due to the reduced internal resistance (Figure 3e), which might be related to the formation of robust and high Li-ion conductive SEI and CEI layer. These results prove that the excellent performance of LMB cells with NFE–$LiNO_3$ can be efficiently improved, accompanied by a safety guarantee compared to the other electrolytes.

To verify the reasons for the excellent cycling performance of the Li||NMC622 cell with NFE–$LiNO_3$, the EIS measurements at specific cycles were performed, and the results are shown in Figure 4(b–d). The equivalent circuit for the impedance spectra and the values for the interface resistance ($R_{Interface} = R_{SEI} + R_{CT}$) are illustrated in Figure S19. The $R_{Interface}$ values of the cells with

© 2022 Wiley-VCH GmbH

25666223, 2023, 2, Downloaded from https://chemistry-europe.onlinelibrary.wiley.com/doi/10.1002/batt.202200453 by University of Ulsan, Wiley Online Library on [11/11/2025]. See the Terms and Conditions (https://onlinelibrary.wiley.com/terms-and-conditions) on Wiley Online Library for rules of use; OA articles are governed by the applicable Creative Commons License

Research Article
doi.org/10.1002/batt.202200453
Chemistry Europe
European Chemical Societies Publishing

NFE–LiPF6 and NFE–LiTFSI dropped after the 1st cycle and suddenly increased after the 10th cycle. This indicates the continuous depletion of electrolyte and the formation of a thick and unstable CEI layer, which in fact can seriously degrade the structure of the cathode and cause the loss of performance to the cells. These results were in agreement with the increase of voltage polarization (Figure S16) and capacity fading (Figure 4a). Conversely, the low interface impedance of the cell with NFE–$LiNO_3$ and the stabilization of this value were achieved after only a few initial cycles to construct sound and stable passivation (SEI/CEI) layers, protecting the cathodes from unwanted reactions, resulting in improved cycling performance.

Characterization of the SEI layer on Li metal anode

The reasons behind the enhanced electrochemical stability in LMBs might be related to the morphologies and components of the SEI/CEI layer forming on the Li metal anode/NMC cathode. To get a deep insight, scanning electron microscopy (SEM) and X-ray photoelectron spectroscopy (XPS) measurements were implemented to probe the structural morphologies and compositions of those layers. The samples were collected from the disassembly of Li||NMC622 cells after 100 cycles and prepared for the SEM and XPS with special care. Figure 5a–e shows the SEM images of the top view and cross-section of the cycled Li anodes. The morphology of Li surfaces taken from the cells with NFE–$LiPF_6$ and NFE–LiTFSI exhibited a loose and

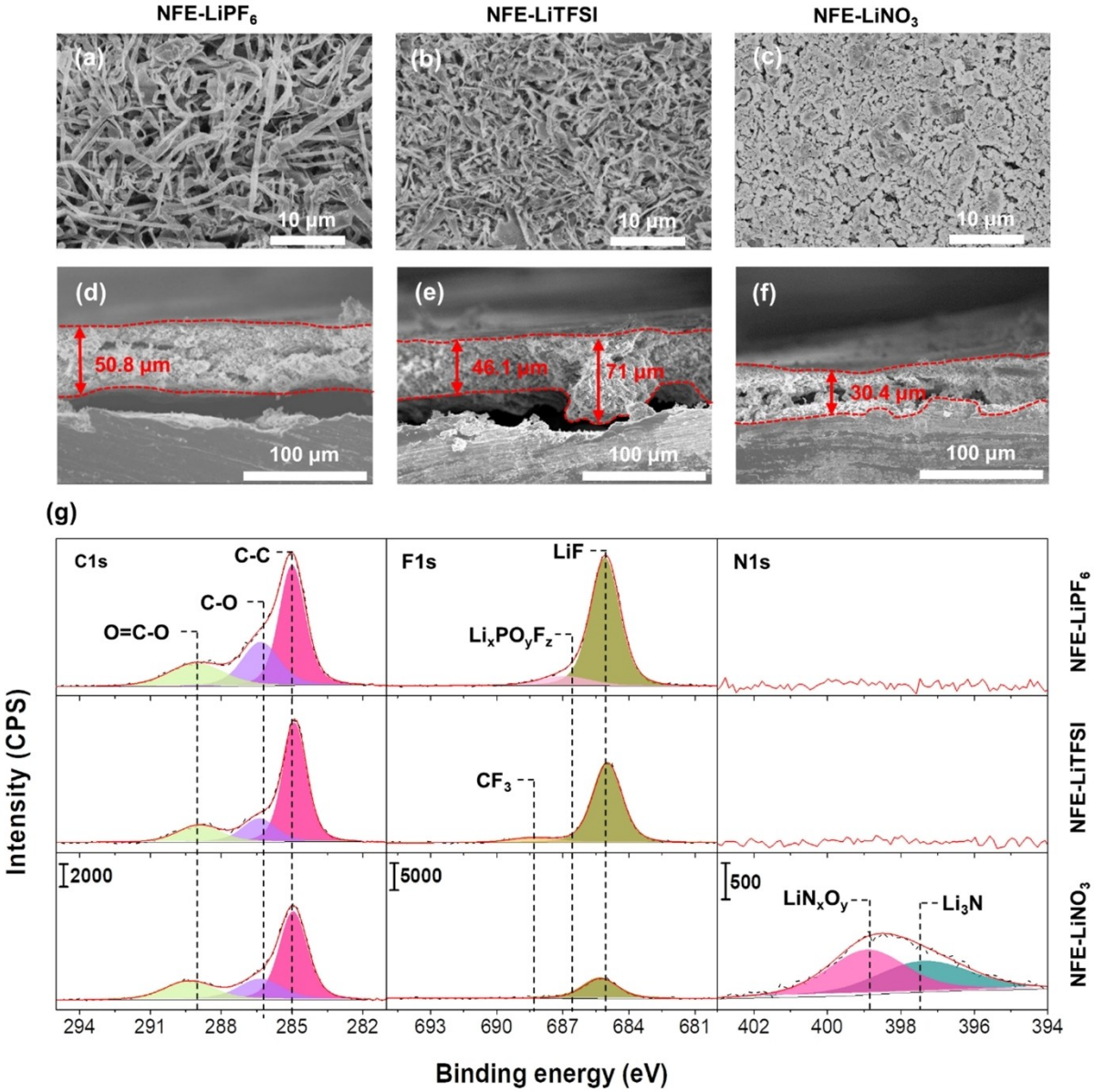

Figure 5. SEM images of the cycled Li metal anodes recovered from Li||NMC622 cell after 100 cycles using NFE–$LiPF_6$, a) top-view and d) cross-section; NFE–LiTFSI, b) top-view and e) cross-section; NFE–$LiNO_3$, c) top-view and f) cross-section. g) The C 1s, F 1s, N 1s XPS spectra of the cycled Li metal anodes recovered from Li||NMC622 cell after 100 cycles in NFE–$LiPF_6$, NFE–LiTFSI, and NFE–$LiNO_3$.

© 2022 Wiley-VCH GmbH

25666223, 2023, 2, Downloaded from https://chemistry-europe.onlinelibrary.wiley.com/doi/10.1002/batt.202200453 by University of Ulsan, Wiley Online Library on [11/11/2025]. See the Terms and Conditions (https://onlinelibrary.wiley.com/terms-and-conditions) on Wiley Online Library for rules of use; OA articles are governed by the applicable Creative Commons License

porous structure, as seen in Figure 5(a and b). The overall surface was heterogeneous with a needle-shaped structure, which might pierce the separator, causing short circuit and safety issues. Given that the formation of SEI layers was unstable and weak, the evolution of morphology on the Li surface cannot be accommodated, resulting in the consumption of electrolytes and fast growth of Li dendrites. These observations were in agreement with the low CEs and large voltage polarization as above-discussed in Figure 3(a and b). In stark contrast, the Li deposited in NFE–$LiNO_3$ showed a homogeneous and dense, with dendrite-free morphology in Figure 5c. The pronounced difference in Li morphologies can be verified by calculating the dendrite nucleation time using Sand's equation.[67] From the equation, it can be inferred that a higher t_{Li^+} will delay the dendrite nucleation time. Therefore, NFE–$LiNO_3$ can effectively suppress the Li dendrite nucleation owing to the high t_{Li^+} (Figure S1b), promoting a uniform and homogeneous Li deposition. Furthermore, the corrosion of Li metal in the NFE–$LiPF_6$ and NFE–LiTFSI was more severe than that in NFE–$LiNO_3$, as obtained from the cross-section images in Figure 5(d and e). After 100 cycles, the thickness of the corroded layers in NFE–$LiPF_6$ and NFE–LiTFSI was observed to be ~50.8 and 46.1–71 μm, respectively. However, the corrosion of the Li anode was effectively restrained using NFE–$LiNO_3$, as evidenced by a thinner layer (~30.4 μm). Based on these results, the effective suppression of the Li dendrite growth and corrosion of Li anode indicated that a highly uniform and stable SEI layer was formed in the NFE–$LiNO_3$, verifying the high CE in Li||Cu cell (Figure 3a), small polarization, and longer Li plating/stripping cycle in the Li||Li symmetric cell (Figure 3b).

To gain a deep insight, XPS measurement was used to investigate the components of the SEI layer formed on the cycled Li metal anode. The binding energies assigned to the deconvoluted peaks of the XPS spectra measured on the surface of Li metal anodes are illustrated in Figure 5(g). In the C 1s spectra, the peak intensity of the C–C (285.0 eV), C–O (286.5 eV), O=C–O (289 eV) was higher in NFE–$LiPF_6$ and NFE–LiTFSI than that in NFE–$LiNO_3$, indicating that abundant organic species was present in the SEI layers. These organic species were mostly originated from the decomposition of the solvent, which was easily dissolved into the electrolyte. Consequently, SEI layers were continuously re-constructed, resulting in severe volumetric expansion of Li metal (Figure 5d and e), and inhibiting the high CE (Figure 3a). Further evidence of more decomposition of electrolyte was found in the O 1s and P 2p spectra, in which strong peaks of C–O (533.5 eV), O=C–O (531.9 eV), P–O (134.3 eV) species were observed in the spectra of NFE–$LiPF_6$ and NFE–LiTFSI (see Figure S20). In the F1s spectra, the formation of different chemical species from the studied electrolytes can be found, that is $Li_xPO_yF_z$ (686.8 eV), $-CF_3$ (688.5 eV), and LiF (685.0 eV). The $Li_xPO_yF_z$ and LiF were the main products that came from the decomposition of $LiPF_6$ salt, whereas the appearance of $-CF_3$ and LiF was related to the decomposition of LiTFSI[5,68] The high LiF content found in NFE–$LiPF_6$ and NFE–LiTFSI might be attributed to the abundant F source in $LiPF_6$ and LiTFSI main salt. Generally, a LiF-rich SEI layer is favorable for stabilizing the Li metal anode, however, too much content can decrease the conductivity of the SEI layer and hamper the Li^+ ion diffusion, resulting in low Li plating/stripping cycles.[69] Interestingly, in the SEI layer generated by NFE–$LiNO_3$, an adequate amount of LiF and various inorganic species such as Li_3N (398 eV), LiN_xO_y (399.5 eV), Li_2O (528.7 eV) species are present (see Figures 5g and S20), suggesting that an inorganic-rich SEI layer induced by the synergetic reaction of both $LiNO_3$ and FEC. The existence of the highly Li-ion conductive species (LiF, Li_2O, Li_3N, and LiN_xO_y) can enhance the kinetics of the Li plating/stripping process, and hence, homogeneous Li deposition can be achieved.[41] Furthermore, less amount of organic species such as O=C–O, C–O, and P–O was detected in O 1s and P 2p, indicating that corrosion reactions between the TEP solvent and Li metal were curbed in NFE–$LiNO_3$. The less generation of organic species and the formation of various inorganic species in NFE–$LiNO_3$ (e.g., LiF, Li_3N, LiN_xO_y, and Li_2O) are highly beneficial for yielding an extremely stable SEI layer. The main reason is attributed to the synergetic effect of $LiNO_3$ and FEC, as confirmed by the previous LSV measurement (Figure S9) and DFT calculation (Figure S10). The crucial formation of an inorganic-rich SEI layer is one of the key factors for the successful suppression of Li dendrite, uniform Li deposition, and consequently, a long Li plating/stripping cycle life.

Characterization of the CEI layer on NMC622 cathode

To further understand the origins behind the superior cycling performance in Ni-rich cathode materials, XPS measurements were performed to probe the components on the surface of cycled NMC622 cathodes. As illustrated in Figure 6(a), in the C 1s spectra, the cathode surface exhibited signals from the conductive carbon (C–C), PVDF binder (CH_2-CF_2), and surface oxide layer (C–O, C=O) of active material (i.e., NMC622). It was found that the intensity of the C–C peak in NFE–$LiPF_6$ and NFE–LiTFSI was significantly lower than that in the pristine NMC622. Although the oxidation potential of all electrolytes investigated here is higher than the operation potential of the NMC material, the oxidation reaction of the electrolytes, especially TEP solvent, still occurs and produces the species covered on the cathode surface. Consequently, the organic-rich CEI layers, which were soluble and unstable, could not give strong protection to the Ni-rich cathode, leading to an irreversible capacity in the cathode, therefore, loss of performance.[5] In contrast, a similar intensity of C–C peak to that of pristine NMC material was detected in the cycled NMC cathode with NFE–$LiNO_3$, revealing the good preservation and electrical connection between the components even after 100 cycles under high voltage (4.3 V). In the F 1s spectra, it can be seen that the LiF (Figure 6a), and the highly Li-ion conductive LiN_xO_y and Li_3N (see Figure S21) species were detected on the cycled NMC622 electrode in NFE–$LiNO_3$, suggesting that more inorganic products generated on the surface of the cathode. This indicates the synergetic participation of $LiNO_3$ and FEC in the formation of a stable CEI layer, directly enhancing the electrochemical performance of the

© 2022 Wiley-VCH GmbH

25666223, 2023, 2, Downloaded from https://chemistry-europe.onlinelibrary.wiley.com/doi/10.1002/batt.202200453 by University of Ulsan, Wiley Online Library on [11/11/2025]. See the Terms and Conditions (https://onlinelibrary.wiley.com/terms-and-conditions) on Wiley Online Library for rules of use; OA articles are governed by the applicable Creative Commons License

Research Article
doi.org/10.1002/batt.202200453
Chemistry Europe
European Chemical Societies Publishing

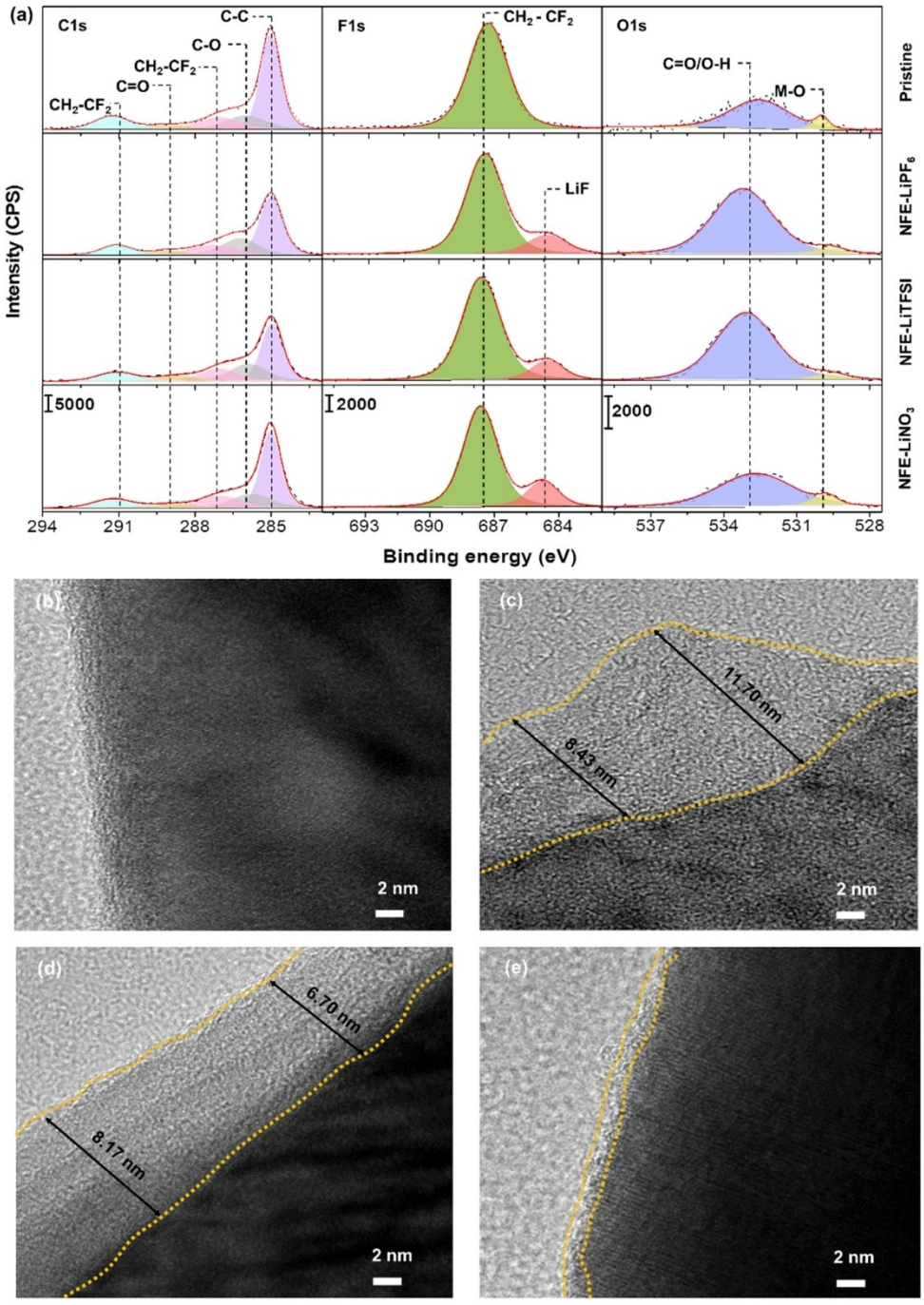

Figure 6. a) The C 1s, F 1s, O 1s XPS spectra of the pristine and cycled NMC622 cathodes recovered from Li||NMC622 cell after 100 cycles in NFE–$LiPF_6$, NFE–LiTFSI, and NFE–$LiNO_3$. TEM images of b) pristine and cycled NMC622 cathodes after 100 cycles in c) NFE–$LiPF_6$, d) NFE–LiTFSI, and e) NFE–$LiNO_3$.

NMC622 cathode. Furthermore, a similar amount of LiF was detected in the F 1s spectrum of the cycled cathodes in the investigated electrolytes (Figure 6a), meaning that the LiF might be derived from the decomposition of the FEC additive. Although the favorable LiF was formed on the cathode surface, the structural integrity of the Ni-rich cathode materials cycled in NFE–$LiPF_6$ and NFE–LiTFSI could not be well-preserved (will be discussed later). In contrast, a robust CEI layer with multi-components generated from $LiNO_3$ and FEC can effectively protect the NMC622 cathode materials by impeding the parasitic reactions of electrolytes to the electrode. Additionally, in the O 1s spectra of NFE–$LiNO_3$, the intensity of the M–O peak (~530 eV), which originated from the transition metal dissolution, was found to be similar to the pristine. This may imply a major difference in the component and thickness of CEI layers, in which the CEI layer formed in NFE–$LiNO_3$ was more uniform, stronger, and thinner than that formed in NFE–$LiPF_6$ and NFE–LiTFSI. The thickness and structure of the CEI layer in

© 2022 Wiley-VCH GmbH

25666223, 2023, 2, Downloaded from https://chemistry-europe.onlinelibrary.wiley.com/doi/10.1002/batt.202200453 by University of Ulsan, Wiley Online Library on [11/11/2025]. See the Terms and Conditions (https://onlinelibrary.wiley.com/terms-and-conditions) on Wiley Online Library for rules of use; OA articles are governed by the applicable Creative Commons License

NFE–$LiNO_3$ were verified by XPS depth-profiling within a range of 0–30 nm (Figures S22–S26) and TEM images (Figure 6b–e). In the C 1s, O 1s, and F 1s spectra of NFE–$LiNO_3$, a negligible change in the C–C, C=O, and CH_2–CF_2 peaks was observed (Figure S22), indicating that the electrode was well-maintained after long cycling. The signal of LiF, LiN_xO_y, and Li_3N in the F 1s and N 1s was detected with high intensity at 0 nm, suggesting that the inorganic species were enriched mostly at the surface. Furthermore, on the cycled NMC cathode in NFE–$LiNO_3$, the detection of a higher amount of LiF than that of the pristine electrode from 3 nm to 30 nm might be attributed to a chemical reaction between PVDF and Li^+ ions, as previously reported.[70,71] However, the increasing amount remained relatively constant with the increase of depth, suggesting that it did not significantly affect the preservation of the electrode during the cycling test. As presented in Figure 6(b–e), the thickness of the CEI layer on the cycled NMC622 cathode in NFE–$LiNO_3$ was estimated at approximately 2 nm, whereas that in NFE–$LiPF_6$ and NFE–LiTFSI was thicker (~11.7 and 8.17 nm, respectively). It is well-known that the serious side reactions between the electrolytes and Ni-rich cathode partially converted the NiO-like layer into the amorphous state via the release of oxygen from the layer lattice,[72] leading to the existence of amorphous materials and thickening of CEI layers. The non-uniform and thick CEI layer covers the NMC622 surface when cycled with NFE–$LiPF_6$ and NFE–LiTFSI, which is unfavorable for the Li-ion transport and the interfacial charge transfer kinetics. On the contrary, the uniform, ultrathin CEI layer formed when cycled in NFE–$LiNO_3$ can result in an advanced performance of the LMB cell, which is also reported in some recent studies.[73,74] Together with the above-mentioned existence of the abundant inorganic species in the CEI layer, a possible formation of polyphosphate on the Ni-rich cathode was also proposed by Yang et al.[39] The polymerization products of TEP (i.e., polyphosphate) induced by nucleophilic moieties can be produced in the CEI layer and are beneficial to the long cycling of LMBs. The protective layer played an important role in suppressing the further oxidative decomposition of the electrolyte, as evidenced by the detection of the polyphosphate only at 0 nm (Figure S26). In conclusion, benefiting from the synergetic combination of $LiNO_3$, FEC and TEP, a robust and Li-ion conductive CEI layer was formed with the existence of abundant inorganic species (LiF, Li_3N and LiN_xO_y) and organic species (polyphosphate). This explains why the formation of a strong CEI layer can prevent further side reactions between electrolyte and cathode and promote the interfacial stability of NMC622 particles during long-term cycling. Moreover, the maintained integrity of the NMC622 cathode cycled in the NFE–$LiNO_3$ was confirmed by cross-section SEM measurements (Figure S27) and XRD analysis (Figure S28) (detailed information can be found in the Supporting Information.). The morphological structure and XRD patterns of the cycled NMC622 secondary particles in NFE–$LiNO_3$ exhibited negligible changes compared to the pristine one, suggesting that the crystalline structure of NMC622 was well-preserved. These results reveal that NFE–$LiNO_3$ enables efficient protection of the integrity of the primary particles and the crystalline structure of NMC622, leading to outstanding battery performance, and hence, it could be a promising candidate for high-voltage LMBs.

Conclusion

In this study, we successfully developed a novel non-flammable electrolyte containing $LiNO_3$ as the main salt, which promotes the concurrent stability of Li metal anode and Ni-rich cathode to achieve an excellent cycling performance in LMBs under high voltage. The solvation structure of $LiNO_3$ in TEP was dominated by the associated ionic species (such as CIPs and AGGs) even at a low concentration, according to Raman spectroscopy and MD simulation. Benefiting from the synergetic effect of $LiNO_3$ and FEC (i.e., the preferential reduction/oxidation) on the Li metal anode/NMC622 cathode, the high quality of SEI and CEI layer was obtained. Furthermore, the merit of TEP solvent was found to be not only non-flammable but also effective in inhibiting the notorious Al corrosion when it was used as the main solvent in the LMB electrolytes. As a result, a high average CE (~97.23%) in the Li||Cu cells and a small polarization (~110 mV) in the Li||Li symmetric cells were obtained. Despite the lower ionic conductivity, NFE–$LiNO_3$ still exhibited exceptional performances in the cells with Ni-rich cathode (Li||NMC622) under 4.3 V, achieving an extremely high average efficiency of ~100% and capacity retention of 90% after 250 cycles. The simultaneous formation of sound SEI and CEI layer efficiently protected both Li metal anode and Ni-rich cathode, improving the Li-ion transport and suppressing the unwanted parasitic reactions between the electrodes and the electrolyte. This was evidenced by the excellent capacity retention and low resistance of cells in NFE–$LiNO_3$ compared to NFE–$LiPF_6$ and NFE–LiTFSI during the cycling tests. Additionally, NFE–$LiNO_3$ can enable the stable cycling of various cathode materials NMC333 and LMO in LMB application.

To summarize, our work presents a facile and effective strategy for solving the dendrite issues associated with Li metal anode and the deterioration of Ni-rich cathode material under high operation voltage. Furthermore, the non-flammable characteristic of NFE–$LiNO_3$ offers a novel approach to handle the safety issues (electrolyte combustion and cell explosion) at the same time. Notably, the remarkable enhancements of the battery performance were achieved by using $LiNO_3$, an economical and easily-synthesized salt, at a low concentration (1 M), effectively reducing the total cost of the formulated electrolyte. The crucial findings of this study indicate that NFE–$LiNO_3$ can be a promising candidate for the next-generation LMBs with prolonged battery life and high safety, giving new guidelines for researchers on the development of the futuristic advanced high-voltage LMBs.

Experimental and computational methods

Detailed information on the experimental and computational procedures can be found in the Supporting Information.

© 2022 Wiley-VCH GmbH

25666223, 2023, 2, Downloaded from https://chemistry-europe.onlinelibrary.wiley.com/doi/10.1002/batt.202200453 by University of Ulsan, Wiley Online Library on [11/11/2025]. See the Terms and Conditions (https://onlinelibrary.wiley.com/terms-and-conditions) on Wiley Online Library for rules of use; OA articles are governed by the applicable Creative Commons License

Acknowledgements

This research was supported by Gunsan City, Korea, under the Human Resources Program for the EV industrial cluster, the National Research Foundation of Korea (NRF) grant funded by the Korea government (MSIT) (NRF-2020R1I1A3066503) and the KAERI Institutional Program (Project No. 522330-22).

Conflict of Interest

The authors declare no conflict of interest.

Data Availability Statement

The data that support the findings of this study are available from the corresponding author upon reasonable request.

Keywords: high voltage · inorganic-rich SEI layer · lithium metal battery · non-flammable · TEP-based electrolyte · ultrathin CEI layer

[1] T. D. Pham, A. Bin Faheem, J. Kim, H. M. Oh, K. Lee, *Small* **2022**, 2107492.
[2] T. D. Pham, A. Bin Faheem, H. D. Nguyen, H. M. Oh, K.-K. Lee, *J. Mater. Chem. A* **2022**, *10*, 12035–12046.
[3] H. V. T. Nguyen, J. Kim, K. K. Lee, *J. Mater. Chem. A* **2021**, *9*, 20725–20736.
[4] T. D. Pham, A. Bin Faheem, S. Y. Chun, J. R. Rho, K. Kwak, K. K. Lee, *Adv. Energy Mater.* **2021**, *11*, 1–17.
[5] T. D. Pham, K. Lee, *Small* **2021**, *2100133*, 2100133.
[6] T. D. Pham, A. Bin Faheem, K. K. Lee, *Small* **2021**, *2103375*, 1–14.
[7] J. Y. Hwang, S. J. Park, C. S. Yoon, Y. K. Sun, *Energy Environ. Sci.* **2019**, *12*, 2174–2184.
[8] S. Chen, F. Dai, M. Cai, *ACS Energy Lett.* **2020**, *5*, 3140–3151.
[9] B. Liu, J. G. Zhang, W. Xu, *Joule* **2018**, *2*, 833–845.
[10] X. Ren, L. Zou, X. Cao, M. H. Engelhard, W. Liu, S. D. Burton, H. Lee, C. Niu, B. E. Matthews, Z. Zhu, C. Wang, B. W. Arey, J. Xiao, J. Liu, J. G. Zhang, W. Xu, *Joule* **2019**, *3*, 1662–1676.
[11] Q. Ma, X. Zhang, A. Wang, Y. Xia, X. Liu, J. Luo, *Adv. Funct. Mater.* **2020**, *30*, 1–8.
[12] Y. Jie, X. Ren, R. Cao, W. Cai, S. Jiao, *Adv. Funct. Mater.* **2020**, *30*, 1910777.
[13] H. Yang, A. Naveed, Q. Li, C. Guo, J. Chen, J. Lei, J. Yang, Y. Nuli, J. Wang, *Energy Storage Mater.* **2018**, *15*, 299–307.
[14] D. Lin, Y. Liu, Y. Cui, *Nat. Nanotechnol.* **2017**, *12*, 194–206.
[15] L. Yu, S. Chen, H. Lee, L. Zhang, M. H. Engelhard, Q. Li, S. Jiao, J. Liu, W. Xu, J.-G. Zhang, *ACS Energy Lett.* **2018**, *3*, 2059–2067.
[16] X. Ren, S. Chen, H. Lee, D. Mei, M. H. Engelhard, S. D. Burton, W. Zhao, J. Zheng, Q. Li, M. S. Ding, M. Schroeder, J. Alvarado, K. Xu, Y. S. Meng, J. Liu, J.-G. Zhang, W. Xu, *Chem* **2018**, *4*, 1877–1892.
[17] S. Chen, J. Zheng, L. Yu, X. Ren, M. H. Engelhard, C. Niu, H. Lee, W. Xu, J. Xiao, J. Liu, J. G. Zhang, *Joule* **2018**, *2*, 1548–1558.
[18] S. Chen, J. Zheng, D. Mei, K. S. Han, M. H. Engelhard, W. Zhao, W. Xu, J. Liu, J.-G. Zhang, *Adv. Mater.* **2018**, *30*, 1706102.
[19] X. Cao, L. Zou, B. E. Matthews, L. Zhang, X. He, X. Ren, M. H. Engelhard, S. D. Burton, P. Z. El-Khoury, H. S. Lim, C. Niu, H. Lee, C. Wang, B. W. Arey, C. Wang, J. Xiao, J. Liu, W. Xu, J. G. Zhang, *Energy Storage Mater.* **2021**, *34*, 76–84.
[20] X. Zhang, L. Zou, Z. Cui, H. Jia, M. H. Engelhard, B. E. Matthews, X. Cao, Q. Xie, C. Wang, A. Manthiram, J.-G. Zhang, W. Xu, *Mater. Today* **2021**, *44*, 15–24.
[21] X. Ren, P. Gao, L. Zou, S. Jiao, X. Cao, X. Zhang, H. Jia, M. H. Engelhard, B. E. Matthews, H. Wu, H. Lee, C. Niu, C. Wang, B. W. Arey, J. Xiao, J. Liu, J. G. Zhang, W. Xu, *Proc. Natl. Acad. Sci. U. S. A.* **2020**, *117*, 28603–28613.
[22] Z. Wang, F. Zhang, Y. Sun, L. Zheng, Y. Shen, D. Fu, W. Li, A. Pan, L. Wang, J. Xu, J. Hu, X. Wu, *Adv. Energy Mater.* **2021**, *2003752*, 1–8.
[23] Z. Wang, Y. Sun, Y. Mao, F. Zhang, L. Zheng, D. Fu, Y. Shen, J. Hu, H. Dong, J. Xu, X. Wu, *Energy Storage Mater.* **2020**, *30*, 228–237.
[24] H. Zhang, W. Qu, N. Chen, Y. Huang, L. Li, F. Wu, R. Chen, *Electrochim. Acta* **2018**, *285*, 78–85.
[25] S. Lee, K. Park, B. Koo, C. Park, M. Jang, H. Lee, H. Lee, *Adv. Funct. Mater.* **2020**, *30*, 1–8.
[26] H. Li, Y. Du, X. Wu, J. Xie, F. Lian, *Adv. Funct. Mater.* **2021**, *31*, 1–10.
[27] K. Liu, X. Li, J. Cai, Z. Yang, Z. Chen, B. Key, Z. Zhang, T. L. Dzwiniel, C. Liao, *ACS Energy Lett.* **2021**, 1315–1323.
[28] S. J. Tan, J. Yue, X. C. Hu, Z. Z. Shen, W. P. Wang, J. Y. Li, T. T. Zuo, H. Duan, Y. Xiao, Y. X. Yin, R. Wen, Y. G. Guo, *Angew. Chemie - Int. Ed.* **2019**, *58*, 7802–7807.
[29] L. Xiao, Z. Zeng, X. Liu, Y. Fang, X. Jiang, Y. Shao, L. Zhuang, X. Ai, H. Yang, Y. Cao, J. Liu, *ACS Energy Lett.* **2019**, *4*, 483–488.
[30] Y. Dong, N. Zhang, C. Li, Y. Zhang, M. Jia, Y. Wang, Y. Zhao, L. Jiao, F. Cheng, J. Xu, *ACS Appl. Energy Mater.* **2019**, *2*, 2708–2716.
[31] Q. Zheng, Y. Yamada, R. Shang, S. Ko, Y. Y. Lee, K. Kim, E. Nakamura, A. Yamada, *Nat. Energy* **2020**, *5*, 291–298.
[32] K. An, Y. H. T. Tran, S. Kwak, J. Han, S. W. Song, *Adv. Funct. Mater.* **2021**, *31*, 1–9.
[33] K. Xu, M. S. Ding, S. Zhang, J. L. Allen, T. R. Jow, *J. Electrochem. Soc.* **2002**, *149*, A622.
[34] Z. L. Brown, S. Heiskanen, B. L. Lucht, *J. Electrochem. Soc.* **2019**, *166*, A2523–A2527.
[35] X. Wang, C. Yamada, H. Naito, G. Segami, K. Kibe, *J. Electrochem. Soc.* **2006**, *153*, A135.
[36] J. K. Feng, X. J. Sun, X. P. Ai, Y. L. Cao, H. X. Yang, *J. Power Sources* **2008**, *184*, 570–573.
[37] H. F. Xiang, Q. Y. Jin, R. Wang, C. H. Chen, X. W. Ge, *J. Power Sources* **2008**, *179*, 351–356.
[38] P. Shi, H. Zheng, X. Liang, Y. Sun, S. Cheng, C. Chen, H. Xiang, *Chem. Commun.* **2018**, *54*, 4453–4456.
[39] H. Yang, Q. Li, C. Guo, A. Naveed, J. Yang, Y. Nuli, J. Wang, *Chem. Commun.* **2018**, *54*, 4132–4135.
[40] J. Yu, Y. Q. Lyu, J. Liu, M. B. Effat, S. C. T. Kwok, J. Wu, F. Ciucci, *J. Mater. Chem. A* **2019**, *7*, 17995–18002.
[41] Z. Wang, Y. Wang, C. Wu, W. K. Pang, J. Mao, Z. Guo, *Chem. Sci.* **2021**, *12*, 8945–8966.
[42] S. Gu, S. Zhang, J. Han, Y. Deng, C. Luo, G. Zhou, Y. He, G. Wei, F. Kang, W. Lv, Q. Yang, *Adv. Funct. Mater.* **2021**, *31*, 2102128.
[43] Y. Liu, D. Lin, Y. Li, G. Chen, A. Pei, O. Nix, Y. Li, Y. Cui, *Nat. Commun.* **2018**, *9*, 1–10.
[44] Q. Shi, Y. Zhong, M. Wu, H. Wang, H. Wang, *Proc. Natl. Acad. Sci. U. S. A.* **2018**, *115*, 5676–5680.
[45] Y. Jie, X. Liu, Z. Lei, S. Wang, Y. Chen, F. Huang, R. Cao, G. Zhang, S. Jiao, *Angew. Chemie - Int. Ed.* **2020**, *59*, 3505–3510.
[46] N. Piao, S. Liu, B. Zhang, X. Ji, X. Fan, L. Wang, P. F. Wang, T. Jin, S. C. Liou, H. Yang, J. Jiang, K. Xu, M. A. Schroeder, X. He, C. Wang, *ACS Energy Lett.* **2021**, *6*, 1839–1848.
[47] S. Liu, X. Ji, N. Piao, J. Chen, N. Eidson, J. Xu, P. Wang, L. Chen, J. Zhang, T. Deng, S. Hou, T. Jin, H. Wan, J. Li, J. Tu, C. Wang, *Angew. Chemie - Int. Ed.* **2021**, *60*, 3661–3671.
[48] S. Liu, J. Mao, W. K. Pang, J. Vongsvivut, X. Zeng, L. Thomsen, Y. Wang, J. Liu, D. Li, Z. Guo, *Adv. Funct. Mater.* **2021**, *31*, 1–11.
[49] G. Zeng, S. Xiong, Y. Qian, L. Ci, J. Feng, *J. Electrochem. Soc.* **2019**, *166*, A1217–A1222.
[50] K. M. Diederichsen, E. J. McShane, B. D. McCloskey, *ACS Energy Lett.* **2017**, *2*, 2563–2575.
[51] H. Zheng, H. Xiang, F. Jiang, Y. Liu, Y. Sun, X. Liang, Y. Feng, Y. Yu, *Adv. Energy Mater.* **2020**, *10*, 1–12.
[52] L. Suo, F. Zheng, Y. S. Hu, L. Chen, *Chinese Phys. B* **2015**, *25*, DOI 10.1088/1674–1056/25/1/016101.
[53] L. Haneke, J. E. Frerichs, A. Heckmann, M. M. Lerner, T. Akbay, T. Ishihara, M. R. Hansen, M. Winter, T. Placke, *J. Electrochem. Soc.* **2020**, *167*, 140526.
[54] R. Xu, X. Shen, X. X. Ma, C. Yan, X. Q. Zhang, X. Chen, J. F. Ding, J. Q. Huang, *Angew. Chemie - Int. Ed.* **2021**, *60*, 4215–4220.
[55] M. P. Andersson, P. Uvdal, *J. Phys. Chem. A* **2005**, *109*, 2937–2941.
[56] I. Phiri, J. Kim, D.-H. Oh, M. Ravi, H.-S. Bae, J. Hong, S. Kim, Y.-C. Jeong, Y. M. Lee, Y.-G. Lee, M.-H. Ryou, *ACS Appl. Mater. Interfaces* **2021**, *13*, 31605–31613.
[57] J. Fu, X. Ji, J. Chen, L. Chen, X. Fan, D. Mu, C. Wang, *Angew. Chemie* **2020**, *132*, 22378–22385.

© 2022 Wiley-VCH GmbH

25666223, 2023, 2, Downloaded from https://chemistry-europe.onlinelibrary.wiley.com/doi/10.1002/batt.202200453 by University of Ulsan, Wiley Online Library on [11/11/2025]. See the Terms and Conditions (https://onlinelibrary.wiley.com/terms-and-conditions) on Wiley Online Library for rules of use; OA articles are governed by the applicable Creative Commons License

[58] G. M. Veith, M. Doucet, R. L. Sacci, B. Vacaliuc, J. K. Baldwin, J. F. Browning, *Sci. Rep.* **2017**, *7*, 6326.
[59] Q. Wang, Z. Yao, C. Zhao, T. Verhallen, D. P. Tabor, M. Liu, F. Ooms, F. Kang, A. Aspuru-Guzik, Y. S. Hu, M. Wagemaker, B. Li, *Nat. Commun.* **2020**, *11*, 1–11.
[60] B. D. Adams, J. Zheng, X. Ren, W. Xu, J.-G. Zhang, *Adv. Energy Mater.* **2018**, *8*, 1702097.
[61] Y. Han, Y. Jie, F. Huang, Y. Chen, Z. Lei, G. Zhang, X. Ren, L. Qin, R. Cao, S. Jiao, *Adv. Funct. Mater.* **2019**, *29*, 1–7.
[62] L. Luo, J. Li, H. Yaghoobnejad Asl, A. Manthiram, *Adv. Mater.* **2019**, *31*, 1–9.
[63] C. Wei, L. Tan, Y. Tao, Y. An, Y. Tian, H. Jiang, J. Feng, Y. Qian, *Energy Storage Mater.* **2021**, *34*, 12–21.
[64] J. Qian, W. A. Henderson, W. Xu, P. Bhattacharya, M. Engelhard, O. Borodin, J. Zhang, *Nat. Commun.* **2015**, *6*, 6362.
[65] A. Abouimrane, J. Ding, I. J. Davidson, *J. Power Sources* **2009**, *189*, 693–696.
[66] S.-I. Pyun, S.-M. Moon, *J. Solid State Electrochem.* **1999**, *3*, 331–336.
[67] P. Bai, J. Li, F. R. Brushett, M. Z. Bazant, *Energy Environ. Sci.* **2016**, *9*, 3221–3229.
[68] P. Shi, L. Zhang, H. Xiang, X. Liang, Y. Sun, W. Xu, *ACS Appl. Mater. Interfaces* **2018**, *10*, 22201–22209.
[69] P. Shi, F. Liu, Y. Z. Feng, J. Zhou, X. Rui, Y. Yu, *Small* **2020**, *16*, 1–8.
[70] D. Leanza, C. A. F. Vaz, P. Novák, M. El Kazzi, *Helv. Chim. Acta* **2021**, *104*, DOI 10.1002/hlca.202000183.
[71] D. Leanza, C. A. F. Vaz, G. Melinte, X. Mu, P. Novák, M. El Kazzi, *ACS Appl. Mater. Interfaces* **2019**, DOI 10.1021/acsami.8b19511.
[72] H. H. Sun, A. Manthiram, *Chem. Mater.* **2017**, *29*, 8486–8493.
[73] X. Zhang, G. Liu, K. Zhou, T. Jiao, Y. Zou, Q. Wu, X. Chen, Y. Yang, J. Zheng, *Energy Mater.* **2021**, *1*, 1–15.
[74] Y. Zou, K. Zhou, G. Liu, N. Xu, X. Zhang, Y. Yang, J. Zhang, J. Zheng, *ACS Appl. Mater. Interfaces* **2021**, *13*, 16427–16436.

Manuscript received: October 14, 2022
Revised manuscript received: November 17, 2022
Accepted manuscript online: November 19, 2022
Version of record online: December 5, 2022

© 2022 Wiley-VCH GmbH

25666223, 2023, 2, Downloaded from https://chemistry-europe.onlinelibrary.wiley.com/doi/10.1002/batt.202200453 by University of Ulsan, Wiley Online Library on [11/11/2025]. See the Terms and Conditions (https://onlinelibrary.wiley.com/terms-and-conditions) on Wiley Online Library for rules of use; OA articles are governed by the applicable Creative Commons License